

Entanglement Dynamics in Two-Qubit Open System Interacting with a Squeezed Thermal Bath via Quantum Nondemolition interaction

Subhashish Banerjee,^{1,2,*} V. Ravishankar,^{1,3,†} and R. Srikanth^{4,1,‡}

¹*Raman Research Institute, Bangalore- 560080, India*

²*Chennai Mathematical Institute, Padur PO, Siruseri 603103, India*

³*Indian Institute of Technology, Kanpur, India*

⁴*Poornaprajna Institute of Scientific Research, Bangalore- 560080, India*

We analyze the dynamics of entanglement in a two-qubit system interacting with its environment via a quantum nondemolition system-reservoir interaction. The system and reservoir are initially assumed to be separable with the reservoir being in an initial squeezed thermal state. Since the resulting dynamics becomes mixed, in order to study the ensuing entanglement, we make use of a recently introduced measure of mixed state entanglement via a probability density function which gives a statistical and geometrical characterization of entanglement by exploring the entanglement content in the various subspaces spanning the two-qubit Hilbert space. After developing the general dynamics, which is categorized into the independent or collective decoherence regime, of N qubits interacting with their bath (reservoir) via a quantum nondemolition interaction we specialize to the two-qubit case for applications. The dynamics is found to satisfy hermiticity and spin-flip symmetry operations. We give an effective temperature dependent dynamics for the collective decoherence regime and make an application of the two-qubit dynamics to a simplified model of quantum repeaters.

PACS numbers: 03.65.Yz, 03.67.Mn, 03.67.Bg, 03.67.Hk

I. INTRODUCTION

Open quantum systems are ubiquitous in the sense that any system can be thought of as being surrounded by its environment (reservoir or bath) which influences its dynamics. They provide a natural route for discussing damping and dephasing. One of the first testing grounds for open system ideas was in quantum optics [1]. Its application to other areas gained momentum from the works of Caldeira and Leggett [2], and Zurek [3], among others. The total Hamiltonian is $H = H_S + H_R + H_{SR}$, where S stands for the system, R for the reservoir and SR for the system-reservoir interaction. The evolution of the system of interest S is studied taking into account the effect of its environment R , through the SR interaction term, making the resulting dynamics non-unitary. Depending upon the system-reservoir ($S - R$) interaction, open systems can be broadly classified into two categories, viz., quantum non-demolition (QND) or dissipative. A particular type of quantum nondemolition (QND) $S - R$ interaction is given by a class of energy-preserving measurements in which dephasing occurs without damping the system, i.e., where $[H_S, H_{SR}] = 0$ while the dissipative systems correspond to the case where $[H_S, H_{SR}] \neq 0$ resulting in decoherence along with dissipation [4].

A class of observables that may be measured repeatedly with arbitrary precision, with the influence of the measurement apparatus on the system being confined strictly to the conjugate observables, is called QND or back-action evasive observables [5, 6, 7, 8]. Such a measurement scheme was originally introduced in the context of the detection of gravitational waves [9, 10]. The energy preserving measurements, referred to above, form an important class of such a general QND measurement scheme.

The interest in the relevance of open system ideas to quantum information has increased in recent times because of the impressive progress made on the experimental front in the manipulation of quantum states of matter towards quantum information processing and quantum communication. Myatt *et al.* [11] and Turchette *et al.* [12] have performed a series of experiments in which they induced decoherence and decay by coupling the atom (their system- S) to engineered reservoirs, in which the coupling to, and the state of, the environment are controllable. An experiment reported in Ref. [13] demonstrated and completely characterized a QND scheme for making a nondeterministic measurement of a single photon nondestructively using only linear optics and photo-detection of ancillary modes, to

*Electronic address: subhashish@cmi.ac.in

†Electronic address: vravi@iitk.ac.in

‡Electronic address: srik@poornaprajna.org

induce a strong nonlinearity at the single photon level. The dynamics of decoherence in continuous atom-optical QND measurements has been studied in [14].

Quantum entanglement is the inherent property of a system to exhibit correlations, the physical basis being the non-local nature of quantum mechanics [15], and hence is a property that is exclusively quantum in nature. Entanglement plays a central role in quantum information theory [16] as in interesting non-classical applications such as quantum computation [17] and quantum error correction [18]. A number of methods have been proposed for creating entanglement involving trapped atoms [19, 20, 21].

An important issue is to study how quantum entanglement is affected by noise, which can be thought of as a manifestation of an open system effect [22]. A recent experimental investigation of the dynamics of entanglement with a continuous monitoring of the environment, i.e., via a realization of quantum trajectories [23], has been made in [24]. Here we study the effect of noise on the entanglement generated between two spatially separated qubits, by means of their interaction with the bath, which is taken to be in an initial squeezed-thermal state [4, 25]. This is of relevance to evaluate the performance of two-qubit gates in practical quantum information processing systems. The two qubits are initially uncorrelated. With the advent of time entanglement builds up between them via their interaction with the bath but eventually gets destroyed because of the quantum to classical transition mediated by the noise. In this paper we study the effect of noise generated by a QND $S - R$ interaction and take up the issue of a dissipative noise in a separate work.

Since we are dealing here with a two qubit system which very rapidly evolves into a mixed state, a study of entanglement would necessarily involve a measure of entanglement for mixed states. Entanglement of a bipartite system in a pure state is unambiguous and well defined. However, mixed state entanglement (MSE) is not so well defined. Thus, although a number of criteria such as entanglement of formation [26, 27, 28] and separability [29] exist, there is a realization [26] that a single quantity is inadequate to describe MSE. This was the principal motivation for the development of a new prescription of MSE [30] in which it is characterized not as a function, but as a probability density function (PDF). The known prescriptions such as concurrence and negativity emerge as particular parameters that characterize the probability density. We will principally make use of this measure in our study of entanglement in the two-qubit system.

The plan of the paper is as follows. In Section II, we give a brief description of the recently developed entanglement measure of MSE [30]. In Sections III and IV, we develop our open system model for the multi-qubit dynamics under the influence of a QND $S - R$ interaction. Section III develops the general dynamics for a multi-qubit system, where the qubits are spatially separated, initially uncorrelated and the bath is in a general squeezed-thermal state. Section IV specializes these considerations to the case of two qubits. In Section V, we point out some interesting symmetries obeyed by the two-qubit dynamics. Section VI deals with the entanglement analysis of the two-qubit open system using the PDF as a measure of entanglement. We also briefly dwell upon the usual measure of MSE, concurrence. We deal with the scenarios where the two qubits effectively interact via localized $S - R$ interactions, called the independent decoherence model, as also when they interact collectively with the bath, called the collective decoherence model. In Section VII, we make a brief discussion of the temperature dependent effective dynamics obeyed by the two-qubit open system in the collective decoherence regime. Section VIII makes a brief application of the model to practical quantum communication, in particular, in the realization of a quantum repeater [31, 32]. In Section IX, we make our conclusions.

II. CHARACTERIZATION OF MIXED STATE ENTANGLEMENT THROUGH A PROBABILITY DENSITY FUNCTION

Here we briefly recapitulate the characterization of mixed state entanglement (MSE) through a PDF as developed in [30]. As pointed out in the Introduction, the above criterion was evolved from the motivation that for the characterization of MSE, a single parameter is inadequate. The basic idea is to express the PDF of entanglement of a given system density matrix (in this case, a two-qubit) in terms of a weighted sum over the PDF's of projection operators spanning the full Hilbert space of the system density matrix. The PDF of a system in a state which is a projection operator $\rho = \frac{1}{M}\Pi_M$ of rank M is defined as:

$$\mathcal{P}_{\Pi_M}(\mathcal{E}) = \frac{\int d\mathcal{H}_{\Pi_M} \delta(\mathcal{E}_\psi - \mathcal{E})}{\int d\mathcal{H}_{\Pi_M}}, \quad (1)$$

where $\int d\mathcal{H}_{\Pi_M}$ is the volume measure for \mathcal{H}_{Π_M} , which is the subspace spanned by Π_M . The volume measure is determined by the invariant Haar measure associated with the group of automorphisms of $\int d\mathcal{H}_{\Pi_M}$, modulo the stabilizer group of the reference state generating \mathcal{H}_{Π_M} . Thus for a one dimensional projection operator, representing a pure state, the group of automorphisms consists of only the identity element and the PDF is simply given by the

Dirac delta. Indeed, if $\rho = \Pi_1 \equiv |\psi\rangle\langle\psi|$, the PDF has the form $\mathcal{P}_\rho(\mathcal{E}) = \delta(\mathcal{E} - \mathcal{E}_\psi)$ thereby resulting in the description of pure state entanglement, as expected, by a single number. The entanglement density of a system in a general mixed state ρ is given by resolving it in terms of nested projection operators with appropriate weights as

$$\begin{aligned} \rho &= (\lambda_1 - \lambda_2)\Pi_1 + (\lambda_2 - \lambda_3)\Pi_2 + \dots(\lambda_{N-1} - \lambda_N)\Pi_{N-1} + \lambda_N\Pi_N \\ &\equiv \sum_{M=1}^N \Lambda_M \Pi_M, \end{aligned} \quad (2)$$

where the projections are $\Pi_M = \sum_{j=1}^M |\psi_j\rangle\langle\psi_j|$, with $M = 1, 2, \dots, N$ and the eigenvalues $\lambda_1 \leq \lambda_2 \leq \dots$, i.e., the eigenvalues are arranged in a non-decreasing fashion. Thus the PDF for the entanglement of ρ is given by

$$\mathcal{P}_\rho(\mathcal{E}) = \sum_{M=1}^N \omega_M \mathcal{P}_{\Pi_M}(\mathcal{E}), \quad (3)$$

where the weights of the respective projections $\mathcal{P}_{\Pi_M}(\mathcal{E})$ are given by $\omega_M = \Lambda_M/\lambda_1$. For a two qubit system, the density matrix would be represented as a nested sum over four projection operators, $\Pi_1, \Pi_2, \Pi_3, \Pi_4$ corresponding to one, two, three and four dimensional projections, respectively, with Π_1 corresponding to a pure state and Π_4 corresponding to a uniformly mixed state, is a multiple of the identity operator. The most interesting structure is present in Π_2 , the two-dimensional projection, which is characterized by three parameters, viz. \mathcal{E}_{cusp} , the entanglement at which the PDF diverges, \mathcal{E}_{max} , the maximum entanglement allowed and $\mathcal{P}_2(\mathcal{E}_{max})$, the PDF corresponding to \mathcal{E}_{max} . The three dimensional projection Π_3 is characterized by the parameter \mathcal{E}_\perp , which parametrizes a discontinuity in the entanglement density function curve. By virtue of the convexity of the sum over the nested projections (2), it can be seen that the concurrence of any state ρ is given by the inequality $\mathcal{C}_\rho \leq (\lambda_1 - \lambda_2)\mathcal{C}_{\Pi_1} + (\lambda_2 - \lambda_3)\mathcal{C}_{\Pi_2}$. Thus while the concurrence for a three and four dimensional projection is identically zero, through the PDF one is able to make a statement about the entanglement content of these spaces. Also, as pointed out in [30], in the case of NMR quantum computation, concurrence and negativity are zero, whereas the PDF is able to elucidate the role of entanglement utilized by the NMR operations. These features as well as the fact that the PDF (3) enables us to study entanglement of a physical state by exploiting the richness inherent in the subspaces spanned by the system Hilbert space makes the PDF an attractive statistical and geometric characterization of entanglement. We provide an explicit illustration of this in Section VI.

III. TWO-QUBIT QND INTERACTION WITH A SQUEEZED THERMAL BATH

We consider the Hamiltonian, describing the QND interaction of L qubits with the bath as [4, 33, 34]

$$\begin{aligned} H &= H_S + H_R + H_{SR} \\ &= \sum_n \hbar \varepsilon_n J_z^n + \sum_k \hbar \omega_k b_k^\dagger b_k + \sum_{n,k} \hbar J_z^n (g_k^n b_k^\dagger + g_k^{n*} b_k). \end{aligned} \quad (4)$$

Here H_S, H_R and H_{SR} stand for the Hamiltonians of the system, reservoir and system-reservoir interaction, respectively. b_k^\dagger, b_k denote the creation and annihilation operators for the reservoir oscillator of frequency ω_k , g_k^n stands for the coupling constant (assumed to be position dependent) for the interaction of the oscillator field with the qubit system and are taken to be

$$g_k^n = g_k e^{-ik \cdot r_n}, \quad (5)$$

where r_n is the qubit position. Since $[H_S, H_{SR}] = 0$, the Hamiltonian (1) is of QND type. In the parlance of quantum information theory, the noise generated is called the phase damping noise [4, 35].

The position dependence of the coupling of the qubits to the bath (5) helps to bring out the effect of entanglement between qubits through the qubit separation: $r_{mn} \equiv r_m - r_n$. This allows for a discussion of the dynamics in two regimes: (A). independent decoherence where $k \cdot r_{mn} \sim \frac{r_{mn}}{\lambda} \geq 1$ and (B). collective decoherence where $k \cdot r_{mn} \sim \frac{r_{mn}}{\lambda} \rightarrow 0$. The case (B) of collective decoherence would arise when the qubits are close enough for them to experience the same environment or when the bath has a long correlation length (set by the effective wavelength λ) compared to the interqubit separation r_{mn} [33]. Our aim is to study the reduced dynamics of the qubit system. As in the case of a single qubit QND interaction with bath [4, 34], the density matrix is evaluated in the system eigenbasis $|i_n\rangle = |\pm \frac{1}{2}\rangle$

(the possible eigenstates of J_z^n with eigenvalues $j_n = \pm \frac{1}{2}$). The system-plus-reservoir composite is closed and hence obeys a unitary evolution given, in the interaction picture, by

$$\rho(t) = U_I(t)\rho(0)U_I^\dagger(t), \quad (6)$$

where

$$U_I(t) = \mathcal{T} e^{-i/\hbar \int_0^t dt' H_I(t')}, \quad (7)$$

with $H_I(t) = e^{i(H_S+H_R)t/\hbar} H_{SR} e^{-i(H_S+H_R)t/\hbar}$, and \mathcal{T} denotes time ordering. Also

$$\rho(0) = \rho^s(0)\rho_R(0), \quad (8)$$

i.e., we assume separable initial conditions. Here

$$\rho^s(0) = \rho_{i_1, j_1}^s(0) \otimes \rho_{i_2, j_2}^s(0) \cdots \otimes \rho_{i_L, j_L}^s(0), \quad (9)$$

is the initial state of the qubit system with $\rho_{i_m, j_m}^s(0) = \langle i_m | \rho^s(0) | j_m \rangle$. In Eq. (8), $\rho_R(0)$ is the initial density matrix of the reservoir which we take to be a squeezed thermal bath [4, 34, 35] given by

$$\rho_R(0) = S(r, \Phi)\rho_{th}S^\dagger(r, \Phi), \quad (10)$$

where

$$\rho_{th} = \prod_k [1 - e^{-\beta\hbar\omega_k}] e^{-\beta\hbar\omega_k b_k^\dagger b_k} \quad (11)$$

is the density matrix of the thermal bath at temperature T , with $\beta \equiv 1/(k_B T)$, k_B being the Boltzmann constant, and

$$S(r_k, \Phi_k) = \exp \left[r_k \left(\frac{b_k^2}{2} e^{-2i\Phi_k} - \frac{b_k^{\dagger 2}}{2} e^{2i\Phi_k} \right) \right] \quad (12)$$

is the squeezing operator with r_k, Φ_k being the squeezing parameters [36].

In order to obtain the reduced dynamics of the system, we trace over the reservoir variables. The matrix elements of the reduced density matrix in the system eigenbasis are obtained for the independent and collective decoherence models as:

A. Independent decoherence model

$$\rho_{\{i_n, j_n\}}^s(t) = \exp[i\{\Theta_{\{i_n, j_n\}}^{\text{in}}(t) - \Lambda_{\{i_n, j_n\}}^{\text{in}}(t)\}] \exp[-\Gamma_{\{i_n, j_n\}}^{\text{in}}(\text{sq})(t)] \rho_{\{i_n, j_n\}}^s(0). \quad (13)$$

Here $\rho_{\{i_n, j_n\}}^s(t)$ stands for $\langle i_L, i_{L-1}, \dots, i_1 | \text{Tr}_R \rho^s(t) | j_L, j_{L-1}, \dots, j_1 \rangle$ and the symbol $\{i_n, j_n\}$ stands collectively for $i_1, j_1; i_2, j_2; \dots; i_L, j_L$. The superscript *in* is to indicate that these expressions are for the independent decoherence model and the subscript *sq* indicates that the bath starts in a squeezed thermal initial state. As seen from the expressions given below, $\Theta_{\{i_n, j_n\}}^{\text{in}}$ and $\Lambda_{\{i_n, j_n\}}^{\text{in}}$ are independent of the bath initial conditions and are given in the continuum limit (assuming a quasi-continuous bath spectrum) by

$$\Theta_{\{i_n, j_n\}}^{\text{in}}(t) = 2 \int_0^\infty d\omega I(\omega) S(\omega, t) \sum_{\substack{m=1, n=2 \\ (m \neq n)}}^L (i_m i_n - j_m j_n) \cos(\omega t_s), \quad (14)$$

$$\Lambda_{\{i_n, j_n\}}^{\text{in}}(t) = 2 \int_0^\infty d\omega I(\omega) C(\omega, t) \sum_{(m \neq n)}^L i_m j_n \sin(\omega t_s). \quad (15)$$

In the above equations, $I(\omega)$ is the bath spectral density which for the Ohmic case considered here has the form

$$I(\omega) = \frac{\gamma_0}{\pi} \omega e^{-\omega/\omega_c}, \quad (16)$$

where γ_0 and ω_c are two bath parameters. Also

$$S(\omega, t) = \frac{\omega t - \sin(\omega t)}{\omega^2}, \quad (17)$$

and

$$C(\omega, t) = \frac{1 - \cos(\omega t)}{\omega^2}. \quad (18)$$

Also in Eqs. (14) and (15), $\omega t_s \equiv k.r_{mn}$ [33]. In Eq. (13) $\Gamma_{sq}^{in}(t)$ is given as

$$\begin{aligned} \Gamma_{\{i_n, j_n\}(sq)}^{in}(t) &= \int_0^\infty d\omega I(\omega) \coth\left(\frac{\beta\hbar\omega}{2}\right) \\ &\times \left[\cosh(2r)C(\omega, t) \left\{ \sum_{m=1}^L (i_m - j_m)^2 + 2 \sum_{\substack{m=1, n=2 \\ (m \neq n)}}^L (i_m - j_m)(i_n - j_n) \cos(\omega t_s) \right\} \right. \\ &- \frac{2}{\omega^2} \sin^2\left(\frac{\omega t}{2}\right) \sinh(2r) \left\{ \cos(\omega(t - 2a)) \left[\sum_{m=1}^L (i_m - j_m)^2 \cos(\omega t_{corr1}) \right. \right. \\ &+ 2 \sum_{\substack{m=1, n=2 \\ (m \neq n)}}^L (i_m - j_m)(i_n - j_n) \cos(\omega t_{corr2}) \left. \right] + \sin(\omega(t - 2a)) \left[\sum_{m=1}^L (i_m - j_m)^2 \sin(\omega t_{corr1}) \right. \\ &\left. \left. + 2 \sum_{\substack{m=1, n=2 \\ (m \neq n)}}^L (i_m - j_m)(i_n - j_n) \sin(\omega t_{corr2}) \right] \right\} \left. \right], \quad (19) \end{aligned}$$

where we have defined two new time scales $\omega t_{corr1} \equiv 2k.r_m$ and $\omega t_{corr2} \equiv k.(r_n + r_m)$ which are due to the non-stationary effects introduced by the squeezed thermal bath. Here we have for simplicity taken the squeezed bath parameters as

$$\begin{aligned} \cosh(2r(\omega)) &= \cosh(2r), \quad \sinh(2r(\omega)) = \sinh(2r), \\ \Phi(\omega) &= a\omega, \end{aligned} \quad (20)$$

where a is a constant depending upon the squeezed bath.

B. Collective decoherence model

The reduced density matrix is given by

$$\rho_{\{i_n, j_n\}}^s(t) = \exp[i\{\Theta_{\{i_n, j_n\}}^{\text{col}}(t) - \Lambda_{\{i_n, j_n\}}^{\text{col}}(t)\}] \exp[-\Gamma_{\{i_n, j_n\}(sq)}^{\text{col}}(t)] \rho_{\{i_n, j_n\}}^s(0). \quad (21)$$

The superscript col is to indicate that these expressions are for the collective decoherence model and the subscript sq indicates that the bath starts in a squeezed thermal initial state. As in the case of independent decoherence, Θ^{col} and Λ^{col} are independent of the bath initial conditions and are given in the continuum limit (assuming a quasi-continuous bath spectrum) by

$$\Theta^{\text{col}}(t) = \int_0^\infty d\omega I(\omega) S(\omega, t) \left[\left(\sum_{m=1}^L i_m \right)^2 - \left(\sum_{m=1}^L j_m \right)^2 \right], \quad (22)$$

$$\Lambda^{\text{col}}(t) = 0. \quad (23)$$

The bath spectral density $I(\omega)$ is as in Eq. (16). In Eq. (21), $\Gamma_{\{i_n, j_n\}(\text{sq})}^{\text{col}}(t)$ is

$$\begin{aligned} \Gamma_{\{i_n, j_n\}(\text{sq})}^{\text{col}}(t) = & \int_0^\infty d\omega I(\omega) \coth\left(\frac{\beta\hbar\omega}{2}\right) \left[\cosh(2r)C(\omega, t) \left[\sum_{m=1}^L (i_m - j_m) \right]^2 \right. \\ & - \frac{2}{\omega^2} \sin^2\left(\frac{\omega t}{2}\right) \sinh(2r) \left\{ \cos(\omega(t-2a)) \left[\sum_{m=1}^L (i_m - j_m)^2 \cos(\omega t_{\text{corr}1}) \right. \right. \\ & + 2 \sum_{\substack{m=1, n=2 \\ (m \neq n)}}^L (i_m - j_m)(i_n - j_n) \cos(\omega t_{\text{corr}2}) \left. \left. + \sin(\omega(t-2a)) \left[\sum_{m=1}^L (i_m - j_m)^2 \sin(\omega t_{\text{corr}1}) \right. \right. \right. \\ & \left. \left. \left. + 2 \sum_{\substack{m=1, n=2 \\ (m \neq n)}}^L (i_m - j_m)(i_n - j_n) \sin(\omega t_{\text{corr}2}) \right] \right\} \right], \quad (24) \end{aligned}$$

All the other terms are as defined above. On comparing Eq. (24) with (19), we find that the terms proportional to $\sinh(2r)$, arising from the non-stationarity of the squeezed bath, are same while the terms proportional to $\cosh(2r)$ differ from each other. For the collective decoherence model, $\omega t_s \equiv k.r_{mn} \equiv 0$, but the two time-scales coming from the non-stationary components of the squeezed thermal bath, i.e., $\omega t_{\text{corr}1} \equiv 2k.r_m$ and $\omega t_{\text{corr}2} \equiv k.(r_n + r_m)$ are both non-zero, indicative of correlations induced between the qubits by the bath squeezing. For the case of zero bath squeezing, both the Eqs. (24) and (19) reduce to their corresponding values for the case of a thermal bath [33].

IV. TWO QUBIT INTERACTION

Here we specialize the general considerations of the previous section to the case of two qubits.

A. Independent decoherence model

The reduced density matrix is a specialization of Eq. (13) to the case of two qubits, say a and b. Here $\rho_{\{i_n, j_n\}}^s(t)$ would be $\rho_{\{i_a, j_b\}}^s(t)$ which represents $\langle i_a, i_b | \text{Tr}_R \rho^s(t) | j_a, j_b \rangle$, where the states $|i_a\rangle$ or $|i_b\rangle$ have eigenvalues $\pm \frac{1}{2}$. We will collectively represent the two-particle index ab by a single 4-level index according to the following scheme:

$$-\frac{1}{2}, -\frac{1}{2} \equiv 0, \quad -\frac{1}{2}, \frac{1}{2} \equiv 1, \quad \frac{1}{2}, -\frac{1}{2} \equiv 2, \quad \frac{1}{2}, \frac{1}{2} \equiv 3.$$

Thus there will be sixteen elements of the density matrix, which we enumerate below. They are seen to satisfy the symmetries:

$$\rho_{32}^s(t) = \rho_{23}^{*s}(t) = \rho_{01}^s(t) = \rho_{10}^{*s}(t), \quad (25)$$

where $*$ in the superscript indicates complex conjugation, and of course the first and last equality follow from the hermiticity of the density operator. In the Eqs. (25), $\Theta_{\{i_n, j_n\}}^{\text{in}}(t)$, $\Lambda_{\{i_n, j_n\}}^{\text{in}}(t)$ can be obtained from the Eqs. (14), (15), respectively, and $\Gamma_{\{i_n, j_n\}(\text{sq})}^{\text{in}}(t)$ from the Eq. (19) and are given by

$$\Theta_{32}^{\text{in}}(t) = \Theta_{01}^{\text{in}}(t) = \int_0^\infty d\omega I(\omega) S(\omega, t) \cos(\omega t_s), \quad (26)$$

$$\Lambda_{32}^{\text{in}}(t) = \Lambda_{01}^{\text{in}}(t) = - \int_0^\infty d\omega I(\omega) C(\omega, t) \sin(\omega t_s), \quad (27)$$

$$\Theta_{23}^{\text{in}}(t) = \Theta_{10}^{\text{in}}(t) = -\Theta_{32}^{\text{in}}(t) = -\Theta_{01}^{\text{in}}(t), \quad (28)$$

$$\Lambda_{23}^{\text{in}}(t) = \Lambda_{10}^{\text{in}}(t) = -\Lambda_{32}^{\text{in}}(t) = -\Lambda_{01}^{\text{in}}(t), \quad (29)$$

and

$$\begin{aligned} \Gamma_{\text{sq}}^{\text{in}}(t) &= \int_0^\infty d\omega I(\omega) \coth\left(\frac{\beta\hbar\omega}{2}\right) \left[\cosh(2r)C(\omega, t) - \frac{2}{\omega^2} \sin^2\left(\frac{\omega t}{2}\right) \sinh(2r) \left\{ \cos(\omega(t-2a)) \cos(\omega t_{\text{corr}1}^{(1)}) \right. \right. \\ &\quad \left. \left. + \sin(\omega(t-2a)) \sin(\omega t_{\text{corr}1}^{(1)}) \right\} \right], \end{aligned} \quad (30)$$

for all the above combinations. In the above equations, ωt_s stands for $k \cdot r_{ab}$ while $\omega t_{\text{corr}1}^{(1)} \equiv 2k \cdot r_b$. Interestingly, for the above cases, the correlation time $\omega t_{\text{corr}2} \equiv k \cdot (r_a + r_b)$ is absent. It can be seen that

$$\rho_{aa}^s(t) = \rho_{aa}^s(0), \quad (a = 0, 1, 2, 3), \quad (31)$$

from which follows that the population remains unchanged. This is a consequence of QND nature of the $S - R$ interaction. Also,

$$\begin{aligned} \rho_{21}^s(t) &= \rho_{12}^{*s}(t) = \rho_{12}^s(t), \\ \rho_{30}^s(t) &= \rho_{03}^{*s}(t) = \rho_{03}^s(t), \end{aligned} \quad (32)$$

i.e., these components are purely real. In the Eqs. (32), $\Theta^{\text{in}}(t)$, $\Lambda^{\text{in}}(t)$ and $\Gamma_{\text{sq}}^{\text{in}}(t)$ are given by

$$\Theta^{\text{in}}(t) = 0 = \Lambda^{\text{in}}(t), \quad (33)$$

and

$$\begin{aligned} \Gamma_{\text{sq},30}^{\text{in}}(t) &= \Gamma_{\text{sq},03}^{\text{in}}(t) = \\ &= \int_0^\infty d\omega I(\omega) \coth\left(\frac{\beta\hbar\omega}{2}\right) \left[2 \cosh(2r)C(\omega, t)[1 + \cos(\omega t_s)] - \frac{2}{\omega^2} \sin^2\left(\frac{\omega t}{2}\right) \sinh(2r) \right. \\ &\quad \times \left\{ \cos(\omega(t-2a))[\cos(2k \cdot r_a) + \cos(2k \cdot r_b) + 2 \cos(k \cdot [r_a + r_b])] \right. \\ &\quad \left. \left. + \sin(\omega(t-2a))[\sin(2k \cdot r_a) + \sin(2k \cdot r_b) + 2 \sin(k \cdot [r_a + r_b])] \right\} \right], \end{aligned} \quad (34)$$

$$\begin{aligned} \Gamma_{\text{sq},21}^{\text{in}}(t) &= \Gamma_{\text{sq},12}^{\text{in}}(t) \\ &= \int_0^\infty d\omega I(\omega) \coth\left(\frac{\beta\hbar\omega}{2}\right) \left[2 \cosh(2r)C(\omega, t)[1 - \cos(\omega t_s)] - \frac{2}{\omega^2} \sin^2\left(\frac{\omega t}{2}\right) \sinh(2r) \right. \\ &\quad \times \left\{ \cos(\omega(t-2a))[\cos(2k \cdot r_a) + \cos(2k \cdot r_b) - 2 \cos(k \cdot [r_a + r_b])] \right. \\ &\quad \left. \left. + \sin(\omega(t-2a))[\sin(2k \cdot r_a) + \sin(2k \cdot r_b) - 2 \sin(k \cdot [r_a + r_b])] \right\} \right]. \end{aligned} \quad (35)$$

Thus we see that the Eqs. (34), (35), depend on both $2k \cdot r_a$ and $2k \cdot r_b$, and $\omega t_{\text{corr}2}$ which is as defined above. Further,

$$\rho_{31}^s(t) = \rho_{13}^{*s}(t) = \rho_{02}^s(t) = \rho_{20}^{*s}(t), \quad (36)$$

where $*$ in the superscript indicates Hermitian conjugation. In the Eqs. (36), $\Theta^{\text{in}}(t)$, $\Lambda^{\text{in}}(t)$ are

$$\Theta_{31}^{\text{in}}(t) = \Theta_{02}^{\text{in}}(t) = \int_0^\infty d\omega I(\omega) S(\omega, t) \cos(\omega t_s), \quad (37)$$

$$\Lambda_{31}^{\text{in}}(t) = \Lambda_{02}^{\text{in}}(t) = \int_0^\infty d\omega I(\omega) C(\omega, t) \sin(\omega t_s), \quad (38)$$

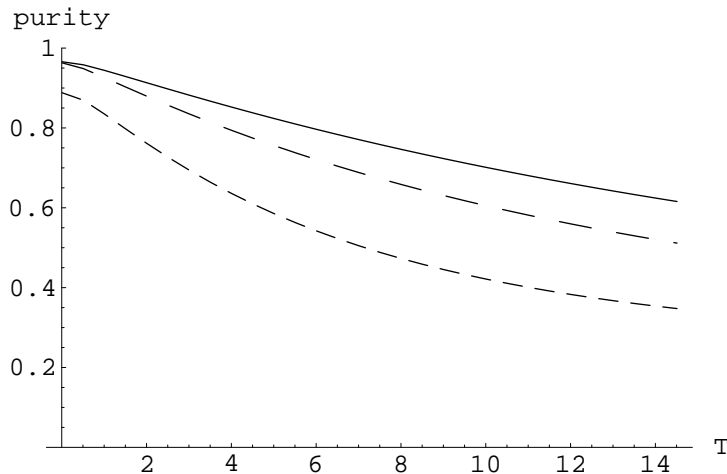


FIG. 1: Purity as a function of temperature T (in units where $\hbar \equiv k_B = 1$) for the independent decoherence model. The bold, large-dashed and small-dashed curves correspond to evolution time $t = 2.0, 3.0$ and 2.0 , respectively. The bath squeezing parameter r (20) is equal to $0.2, 0.2$ and 1.0 , respectively, for the three curves. Here and in all the subsequent figures, the squeezing parameter a (20) is set equal to zero. Also the bath parameters γ_0, ω_c (16) are equal to 0.01 and 100.0 , respectively. All the inter-qubit distances are defined on the scale of the resonant wavelength coming from the wavevector k (5) as a result of the position dependent couplings of the qubits with the bath. In all the plots concerned with the independent decoherence model, kr_{12} is set equal to 1.1 .

$$\Theta_{13}^{\text{in}}(t) = \Theta_{20}^{\text{in}}(t) = -\Theta_{31}^{\text{in}}(t) = -\Theta_{02}^{\text{in}}(t), \quad (39)$$

$$\Lambda_{13}^{\text{in}}(t) = \Lambda_{20}^{\text{in}}(t) = -\Lambda_{31}^{\text{in}}(t) = -\Lambda_{02}^{\text{in}}(t), \quad (40)$$

and

$$\Gamma_{\text{sq}}^{\text{in}}(t) = \int_0^{\infty} d\omega I(\omega) \coth\left(\frac{\beta\hbar\omega}{2}\right) \left[\cosh(2r)C(\omega, t) - \frac{2}{\omega^2} \sin^2\left(\frac{\omega t}{2}\right) \sinh(2r) \left\{ \cos(\omega(t-2a)) \cos(\omega t_{\text{corr}1}^{(2)}) \right. \right. \\ \left. \left. + \sin(\omega(t-2a)) \sin(\omega t_{\text{corr}1}^{(2)}) \right\} \right], \quad (41)$$

for all the above combinations. In the above equations, ωt_s stands for $k \cdot r_{ab}$ while $\omega t_{\text{corr}1}^{(2)} \equiv 2k \cdot r_a$. Interestingly, for the above cases, the correlation time $\omega t_{\text{corr}2} \equiv k \cdot (r_a + r_b)$ is absent. The Eqs. (25), (31), (32) and (36) cover all the density matrices for the two-qubit independent decoherence model.

Figure (1) depicts the behavior of purity, defined here as $\text{Tr}(\rho^2(t))$ for $\rho(t)$ as obtained in this subsection for the independent decoherence model, as a function of temperature T for various evolution times and bath squeezing r (20). In all the figures in this article, we consider the initial state to be an equal superposition state, which can be obtained by applying $H \otimes H$ on the state $|0\rangle \equiv |-\frac{1}{2}, -\frac{1}{2}\rangle$, where H is the Hadamard transformation. It can be seen that with the increase in temperature, as also evolution time t and bath squeezing r , the system becomes more mixed and hence loses its purity.

B. Collective decoherence model

The reduced density matrix is a specialization of Eq. (21) to the case of two qubits, say a and b. The notations are as before.

$$\rho_{32}^s(t) = \rho_{23}^{*s}(t) = \rho_{01}^s(t) = \rho_{10}^{*s}(t), \quad (42)$$

where $*$ in the superscript indicates Hermitian conjugation. In the Eqs. (42), $\Theta^{\text{col}}(t), \Lambda^{\text{col}}(t) (= 0)$ are obtained from the Eqs. (22), (23), respectively and $\Gamma_{\text{sq}}^{\text{col}}(t)$ from Eq. (24). They are given by

$$\Theta_{32}^{\text{in}}(t) = \Theta_{01}^{\text{in}}(t) = \int_0^{\infty} d\omega I(\omega) S(\omega, t), \quad (43)$$

$$\Theta_{23}^{\text{col}}(t) = \Theta_{10}^{\text{col}}(t) = -\Theta_{32}^{\text{col}}(t) = -\Theta_{01}^{\text{col}}(t), \quad (44)$$

and $\Gamma_{\text{sq}}^{\text{col}}(t)$ is as in Eq. (30) for all the cases in Eq. (42), with $\omega t_{\text{corr}1}$ and $\omega t_{\text{corr}2}$ as defined there. As before,

$$\rho_{aa}^s(t) = \rho_{aa}^s(0), \quad (a = 0, 1, 2, 3). \quad (45)$$

This is indicative of QND nature of the $S - R$ interaction which preserves the population. Also,

$$\begin{aligned} \rho_{21}^s(t) &= \rho_{12}^{*s}(t) = \rho_{12}^s(t), \\ \rho_{30}^s(t) &= \rho_{03}^{*s}(t) = \rho_{03}^s(t). \end{aligned} \quad (46)$$

In the Eqs. (46), $\Theta^{\text{col}}(t)$, $\Lambda^{\text{col}}(t)$ and $\Gamma_{\text{sq}}^{\text{col}}(t)$ are given by

$$\Theta^{\text{col}}(t) = 0 = \Lambda^{\text{col}}(t), \quad (47)$$

and

$$\begin{aligned} \Gamma_{\text{sq},30}^{\text{col}}(t) &= \Gamma_{\text{sq},03}^{\text{col}}(t) \\ &= \int_0^\infty d\omega I(\omega) \coth\left(\frac{\beta\hbar\omega}{2}\right) \left[4 \cosh(2r)C(\omega, t) - \frac{2}{\omega^2} \sin^2\left(\frac{\omega t}{2}\right) \sinh(2r) \right. \\ &\quad \times \left\{ \cos(\omega(t-2a))[\cos(2k \cdot r_a) + \cos(2k \cdot r_b) + 2 \cos(k \cdot [r_a + r_b])] \right. \\ &\quad \left. \left. + \sin(\omega(t-2a))[\sin(2k \cdot r_a) + \sin(2k \cdot r_b) + 2 \sin(k \cdot [r_a + r_b])] \right\} \right], \end{aligned} \quad (48)$$

$$\begin{aligned} \Gamma_{\text{sq},21}^{\text{col}}(t) &= \Gamma_{\text{sq},12}^{\text{col}}(t) \\ &= -2 \int_0^\infty \frac{d\omega}{\omega^2} I(\omega) \coth\left(\frac{\beta\hbar\omega}{2}\right) \sin^2\left(\frac{\omega t}{2}\right) \sinh(2r) \\ &\quad \times [\cos(\omega(t-2a))[\cos(2k \cdot r_a) + \cos(2k \cdot r_b) - 2 \cos(k \cdot [r_a + r_b])] \\ &\quad + \sin(\omega(t-2a))[\sin(2k \cdot r_a) + \sin(2k \cdot r_b) - 2 \sin(k \cdot [r_a + r_b])]]. \end{aligned} \quad (49)$$

It is interesting to note from Eqs. (46), (47) and (49), that for the case of a purely thermal bath with zero bath squeezing, $\Gamma_{\text{sq},21}^{\text{col}}(t) = \Gamma_{\text{sq},12}^{\text{col}}(t) = 0$, thereby implying that for these cases, the corresponding density matrix elements do not decay even though they are interacting with the bath. Also, since in a QND $S - R$ interaction, the diagonal terms $\rho_{1,1}$ and $\rho_{2,2}$ do not change, this implies that any state $\alpha|1\rangle + \beta|2\rangle$ in the subspace span $\{|1\rangle, |2\rangle\}$ remains invariant, thereby leading to a *decoherence-free subspace*. This behavior is not retained, in general, for the case of a squeezed thermal bath. However, since a thermal bath is the asymptotic limit of a squeezed thermal bath [37, 38, 39], decoherence-free subspaces emerge asymptotically. Further,

$$\rho_{31}^s(t) = \rho_{13}^{*s}(t) = \rho_{02}^s(t) = \rho_{20}^{*s}(t), \quad (50)$$

where $*$ in the superscript indicates complex conjugation. In Eq. (50), $\Theta^{\text{col}}(t)$, $\Lambda^{\text{col}}(t) (= 0)$ are

$$\Theta_{31}^{\text{col}}(t) = \Theta_{02}^{\text{col}}(t) = \int_0^\infty d\omega I(\omega) S(\omega, t), \quad (51)$$

$$\Theta_{13}^{\text{col}}(t) = \Theta_{20}^{\text{col}}(t) = -\Theta_{31}^{\text{col}}(t) = -\Theta_{02}^{\text{col}}(t), \quad (52)$$

and $\Gamma_{\text{sq}}^{\text{col}}(t)$ is as in Eq. (30), with $2k \cdot r_b \rightarrow 2k \cdot r_a$. The Eqs. (42), (45), (46) and (50) cover all the density matrices for the two-qubit collective decoherence model.

Figure (2) depicts the behavior of purity, defined here as $\text{Tr}(\rho^2(t))$ for $\rho(t)$ as obtained in this subsection for the collective decoherence model, as a function of temperature T for various evolution times and bath squeezing r (20). As before, it can be seen that with the increase in temperature, as also evolution time t and bath squeezing r , the system becomes more mixed and hence loses its purity.

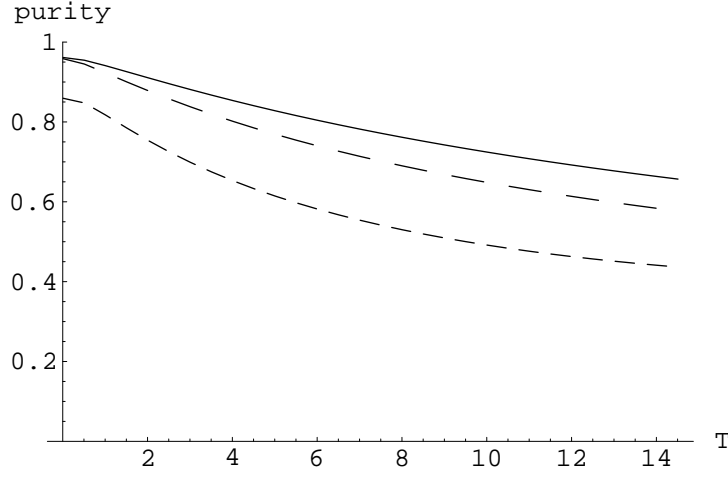


FIG. 2: Purity as a function of temperature T (in units where $\hbar \equiv k_B = 1$) for the collective decoherence model. The bold, large-dashed and small-dashed curves correspond to evolution time $t = 2.0, 3.0$ and 2.0 , respectively. The bath squeezing parameter r (20) is equal to $0.2, 0.2$ and 1.0 , respectively, for the three curves. All the inter-qubit distances are defined on the scale of the resonant wavelength coming from the wavevector k (5) as a result of the position dependent couplings of the qubits with the bath. In all the plots concerned with the collective decoherence model, kr_{12} is set equal to 0.05 .

V. SYMMETRIES IN THE DYNAMICAL SYSTEM

In this section we consider the twoqubit evolution, developed in the previous section from the point of view of some fundamental symmetries. This enables us to view the dynamics from a fresh perspective and is also interesting from its own point of view.

Employing the two-particle index notation used in the previous section, we find that the transformation connecting the initial and final density operations can be given by the following operation

$$\rho_{ab}(t) = \mathcal{L}_{ab}(t)\rho_{ab}(0). \quad (53)$$

The non-trivial aspect of the dynamics that this relation represents is that here \mathcal{L} represents, not a matrix, but a two-dimensional array, and the multiplication is done element-wise.

The most general array \mathcal{L} that satisfies the symmetry, following only from the hermiticity of $\rho(0)$ and $\rho(t)$ is:

$$\mathcal{L} = \begin{pmatrix} 1 & c_1 & c_2 & c_3 \\ c_1^* & 1 & c_4 & c_5 \\ c_2^* & c_4^* & 1 & c_6 \\ c_3^* & c_5^* & c_6^* & 1 \end{pmatrix} \quad (54)$$

However, further constraints on the structure of \mathcal{L} appear because the dynamical evolution due to QND interaction respects spin-flip symmetry (see Eq. (59) below), which is for example (given for clarity, in the single-qubit notation):

$$\mathcal{L}_{\frac{1}{2}, -\frac{1}{2}; \frac{1}{2}, \frac{1}{2}} = \mathcal{L}_{-\frac{1}{2}, \frac{1}{2}; -\frac{1}{2}, -\frac{1}{2}}. \quad (55)$$

This has the effect that c_3 and c_4 are real, which we denote by r_1 and r_2 respectively. Further $c_2 = c_5^*$ and $c_1 = c_6^*$. These are seen by noting that:

$$\begin{aligned} c_3 &\equiv \mathcal{L}_{e,g} = \mathcal{L}_{g,e}^* = \mathcal{L}_{g,e} = \mathcal{L}_{e,g}^* \equiv c_3^*, \\ c_4 &\equiv \mathcal{L}_{s,a} = \mathcal{L}_{a,s}^* = \mathcal{L}_{a,s} = \mathcal{L}_{s,a}^* \equiv c_4^*, \\ c_2 &\equiv \mathcal{L}_{e,a} = \mathcal{L}_{a,e}^* = \mathcal{L}_{g,s} = \mathcal{L}_{s,g}^* \equiv c_5^*, \\ c_1 &\equiv \mathcal{L}_{e,s} = \mathcal{L}_{s,e}^* = \mathcal{L}_{g,a} = \mathcal{L}_{a,g}^* \equiv c_6^*, \end{aligned} \quad (56)$$

where the first and third equalities in each equation follow from hermiticity. Accordingly, Eq. (54) can be rewritten as:

$$\mathcal{L} = \begin{pmatrix} 1 & c_1 & c_2 & r_1 \\ c_1^* & 1 & r_2 & c_2^* \\ c_2^* & r_2 & 1 & c_1^* \\ r_1 & c_2 & c_1 & 1 \end{pmatrix}, \quad (57)$$

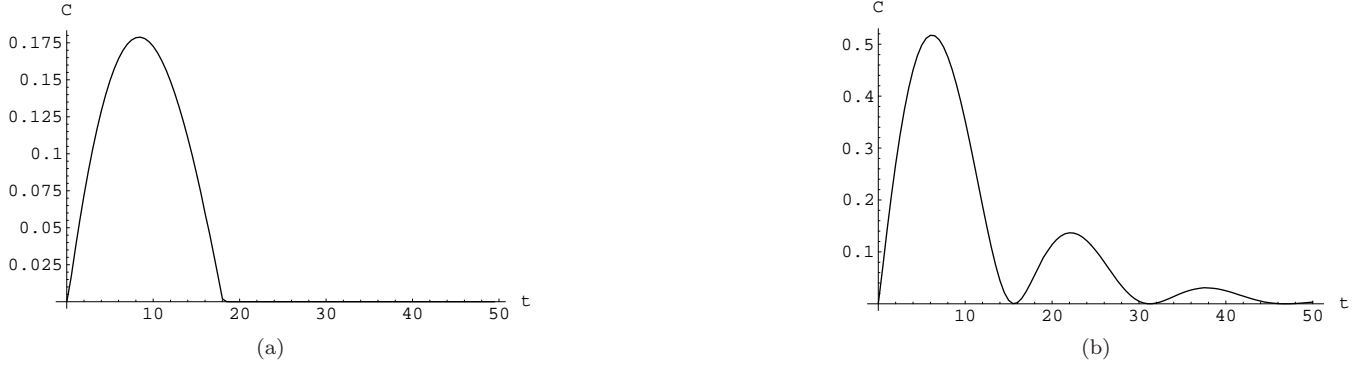


FIG. 3: Concurrence \mathcal{C} (60) as a function of time of evolution t at $T = 5.0$ and bath squeezing parameter r (20) equal to 0.2. Figure (a) refers to the independent decoherence model and (b) the collective decoherence model.

Consider the operator $\hat{\mathcal{L}}$ corresponding to $\mathcal{L}_{j,k}$, defined by:

$$\hat{\mathcal{L}} = \sum_{j,k} \mathcal{L}_{j,k} |j\rangle\langle k|, \quad (j, k = 0, 1, 2, 3). \quad (58)$$

The spin-flip symmetry can be represented by

$$\Sigma \hat{\mathcal{L}} \Sigma^\dagger = \hat{\mathcal{L}}, \quad \Sigma = \sigma_x \otimes \sigma_x. \quad (59)$$

Since $\Sigma = (-i\sigma_x) \otimes (i\sigma_x)$, the above spin-flip symmetry may be described as a rotational symmetry, with angle $\pi/2$ (resp. $3\pi/2$) in the first (resp. second) qubit coordinate about the x -axis.

VI. ENTANGLEMENT ANALYSIS

In this section, we will study the development of entanglement in the two qubit system, both for the independent as well as the collective decoherence model. A well known measure of MSE is the concurrence [27] defined as

$$\mathcal{C} = \max(0, \sqrt{\lambda_1} - \sqrt{\lambda_2} - \sqrt{\lambda_3} - \sqrt{\lambda_4}), \quad (60)$$

where λ_i are the eigenvalues of the matrix

$$R = \rho \tilde{\rho}, \quad (61)$$

with $\tilde{\rho} = \sigma_y \otimes \sigma_y \rho^* \sigma_y \otimes \sigma_y$ and σ_y is the usual Pauli matrix. \mathcal{C} is zero for unentangled states and one for maximally entangled states.

In figure (3 (a)), we plot the concurrence (60) with respect to time for the case of the independent decoherence model, while figure (3 (b)) depicts the temporal behavior of concurrence for the collective decoherence model. It is clearly seen from the figures that the two qubit system is initially unentangled, but with time there is a build up of entanglement between them as a result of their interaction with the bath. Also the entanglement builds up more quickly in the collective decoherence model when compared to the independent model. This is expected as the effective interaction between the two qubits is stronger in the collective case.

Now we take up the issue of entanglement from the perspective of the PDF as in Eq. (3). In figures (4 (a)) and (b), we plot the weights $\omega_1, \omega_2, \omega_3$ and ω_4 (3) of the entanglement densities of the projection operators of the various subspaces which span the two qubit Hilbert space with respect to T for the independent and collective decoherence models, respectively. Since ω_1 is the weight for the one dimensional projection and hence a pure state and ω_4 that of the maximally mixed state with ω_2 and ω_3 being intermediary, these plots depict the variation in the contribution of the various subspaces to the entanglement of the two qubit system as T increases. As can be seen from both the figures, with increase in temperature T , the weight ω_1 , depicting the pure state component monotonically decreases, while the other weights start from zero at $T = 0$ and increase. Eventually, the weight ω_4 depicting a maximally mixed state would be expected to dominate, though for the parameter range used in the plots, this feature is not seen. This feature of the dynamics of the reduced two-qubit system, specially in the case of the collective decoherence model,

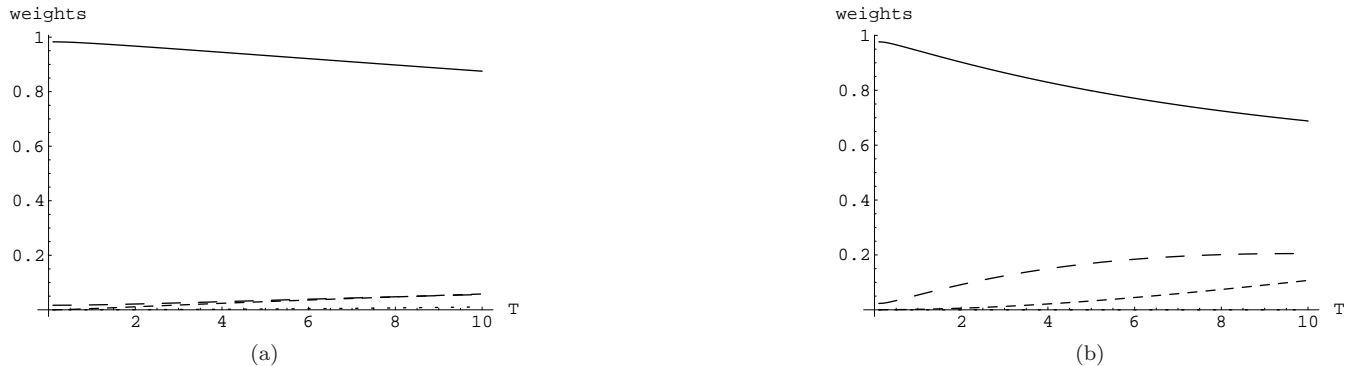


FIG. 4: The weights (3) as a function of T , with an evolution time $t = 5$ and bath squeezing parameter r (20) equal to 0.2. Figure (a) refers to the independent decoherence model and (b) the collective decoherence model. In both the figures, the bold curve corresponds to the weight ω_1 , while the large-dashed, small-dashed and dotted curves correspond to the weights ω_2 , ω_3 and ω_4 , respectively.

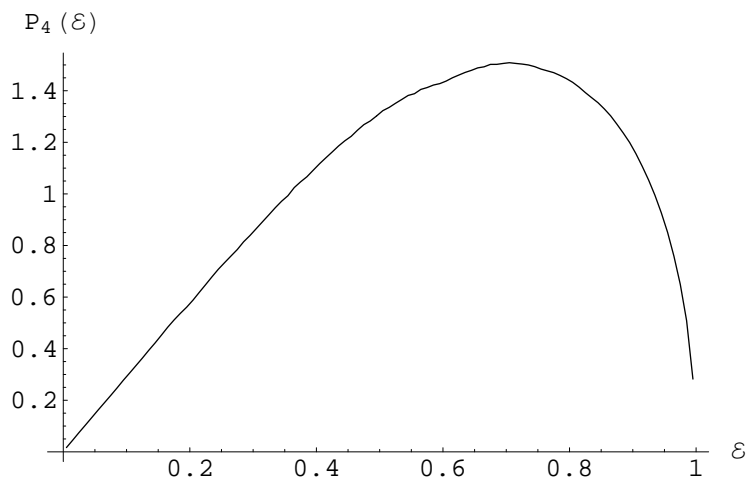


FIG. 5: The PDF for the four dimensional projection spanning the full Hilbert space $\mathcal{H}(\Pi_4)$.

has an interesting application which will be discussed in detail in Section VII where it will be seen to obey an *effective* temperature dependent Hamiltonian, bringing out the persistence of entanglement even at finite temperatures. In the case of the collective decoherence model, the weights ω_2 and ω_3 have a greater growth than that for the independent decoherence model, depicting the greater entanglement development in the collective model as is also borne out by the concurrence plots in figure (3).

As explained in Section II, the characterization of MSE for a two qubit system via the PDF involves the distribution functions of four projection operators, Π_1 , Π_2 , Π_3 , Π_4 corresponding to one, two, three and four dimensional projections, respectively. These will be represented here as $\mathcal{P}_1(\mathcal{E})$, $\mathcal{P}_2(\mathcal{E})$, $\mathcal{P}_3(\mathcal{E})$ and $\mathcal{P}_4(\mathcal{E})$, respectively. Also, as discussed above, $\mathcal{P}_4(\mathcal{E})$ would be universal for the two qubit density matrices and would involve the Haar measure on $SU(4)$ [40]. This is depicted in figure (5) and is common to all the two qubit PDF of entanglement.

Now we consider the $\mathcal{P}_2(\mathcal{E})$ and $\mathcal{P}_3(\mathcal{E})$ density functions for some representative states of the two qubit system, both for the independent as well as collective decoherence models. This enables us to compare the entanglement in the respective subspaces of the system Hilbert space. We also plot the full entanglement density function curve $\mathcal{P}(\mathcal{E})$ with respect to the entanglement \mathcal{E} , at a particular time t . This will enable us to look at the contribution to the entanglement from the different projections.

Figures (6 (a)) and (b) depict the behavior of the density function $\mathcal{P}_2(\mathcal{E})$ for the bath evolution time $t = 2.0$ and $T = 5.0$ for the independent and collective decoherence models, respectively. For these conditions, the value of concurrence (60) is 0.18 for the case of the independent decoherence model and 0.27 for the collective model, depicting the greater entanglement content in the later compared to the former. This is also borne out by these figures. As shown in [30], the concurrence for a two dimensional projection is $\mathcal{C}_{\Pi_2} = (\mathcal{E}_{max} - \mathcal{E}_{cusp})/2$. Thus while

the figure (6 (a)) has $\mathcal{E}_{max} = \mathcal{E}_{cusp}$, resulting in $\mathcal{C}_{\Pi_2} = 0$, it is finite for the case of figure (6 (b)) , thereby reflecting the greater entanglement content in the collective model. Figures (7 (a)) and (b) depict the behavior of the density function $\mathcal{P}_3(\mathcal{E})$ for the bath evolution time $t = 2.0$ and $T = 5.0$ for the independent and collective decoherence models, respectively. In figure (7 (a)), the parameter \mathcal{E}_\perp is ≈ 0.19 while it is one for the collective model as depicted in figure (7 (b)). Since \mathcal{E}_\perp is evaluated from the state perpendicular to the third non-separable basis in the canonical basis of a three dimensional projection [30], this clearly brings out the greater entanglement content in the collective model as compared to the independent case. In figures (8 (a)) and (b), we depict the full density function $\mathcal{P}(\mathcal{E})$ for the independent and collective decoherence models, respectively and with the same parameters as above. This is obtained by a weighted sum over all the contributions of the projection operators from the different subspaces (3). Here and in all the subsequent figures for the full PDF, the contribution from the one dimensional projection Π_1 , which is a delta function, is represented by a line of height equal to its weight (3) and the point on the abscissa is determined by its corresponding entanglement. The figures clearly indicate, that for the given bath parameters and evolution time, the system is still possessed with considerable entanglement, which is clearly greater in the collective case because of the contribution to the full PDF coming almost exclusively from the entanglement in the one dimensional projection.

Figures (9 (a)) and (b) exhibit the behavior of the density function $\mathcal{P}_2(\mathcal{E})$ for the bath evolution time $t = 10.0$ and $T = 5.0$ for the independent and collective decoherence models, respectively. This thus depicts a situation where the two qubit system has been exposed to the bath for a longer time. For these conditions, concurrence (60) is 0.17 for the case of the independent decoherence model and 0.35 for the collective model, showing greater entanglement content in the later compared to the former and also indicating a buildup of entanglement with time. As in the corresponding case before, figure (9 (a)) has $\mathcal{E}_{max} = \mathcal{E}_{cusp}$, resulting in $\mathcal{C}_{\Pi_2} = 0$, while it is finite for the case of figure (9 (b)) , thereby reflecting greater entanglement content in the collective model. Figures (10 (a)) and (b) depict the behavior of the density function $\mathcal{P}_3(\mathcal{E})$ for the bath evolution time $t = 10.0$ and $T = 5.0$ for the independent and collective decoherence models, respectively. In figure (10 (a)), the parameter \mathcal{E}_\perp is ≈ 0.79 while it is one for the collective model as in figure (10 (b)) bringing out greater entanglement content in the collective model in comparison with the independent case. In figures (11 (a)) and (b), the full density function $\mathcal{P}(\mathcal{E})$ is given for the independent and collective decoherence models, respectively and with the same parameters as above. The point on the abscissa, for the one dimensional projection, can be clearly seen to have shifted to the right as compared to the corresponding case in the figures (8 (a)) and (b), thereby indicating a buildup of entanglement with time. Also when compared to figures (8 (a)) and (b), the full PDF as in figures (11 (a)) and (b) exhibit a richer structure which is a consequence of the additional contribution to the full PDF from the two and three dimensional projections. The fourth dimensional projection has an insignificant contribution for the given parameters.

Figures (12 (a)) and (b) give the full density function $\mathcal{P}(\mathcal{E})$ for the independent and collective decoherence models, respectively with a bath evolution time $t = 10.0$ and $T = 50.0$. For these conditions, the value of concurrence (60) is 0, which would indicate a complete breakdown of entanglement. This would be expected as with the increase in the bath temperature T , the effect of entanglement would be destroyed quickly. This is partially borne out by the fact that for this case $\mathcal{C}_{\Pi_2} = 0$. However, as seen from figure (12 (b)), the PDF for the full density function still exhibits a rich entanglement structure, coming principally from the contributions from the one and three dimensional projections. In contrast , figure (12 (a)), for the independent decoherence model, exhibits the Harr measure on $SU(4)$ and thus represents a maximally mixed state.

Figure (13) represents the full density function $\mathcal{P}(\mathcal{E})$ for the independent decoherence model with an evolution time $t = 10.0$, $T = 20.0$ and bath squeezing parameter r equal to 0.2. This would be analogous to that discussed in [30] for NMR quantum computation where concurrence would be zero, and the excess of entangled states over the unpolarized background (exhibited by the uniform distribution coming from the density function Π_4 , related to the four dimensional projection) is exploited as a resource allowing for non-trivial gate operations, thus depicting pseudopure states over the four dimensional background, with the excess being the “deviation density matrix”.

VII. EFFECTIVE TEMPERATURE DEPENDENT DYNAMICS IN THE COLLECTIVE DECOHERENCE MODEL: A BRIEF DISCUSSION

In a QND $S - R$ interaction, the reduced density matrix of the system does not approach a unique distribution asymptotically [4]. As seen from figure (12 (b)), the PDF for the full density function (for the collective decoherence model) exhibits a rich entanglement structure, coming principally from the contributions from the one and three dimensional projections which carry equal weights. This feature is seen to persist for higher temperatures and evolution times, for the collective decoherence model, with the weights of the subspaces spanned by the four projection operators of the PDF remaining intact. From this emerges the fact that for the collective decoherence model, studied here, as the effect of the bath on the system increases, the PDF instead of becoming uniform, as expected, gets distributed between the subspaces spanned by the one and three dimensional projection operators suggesting a tendency of the system to

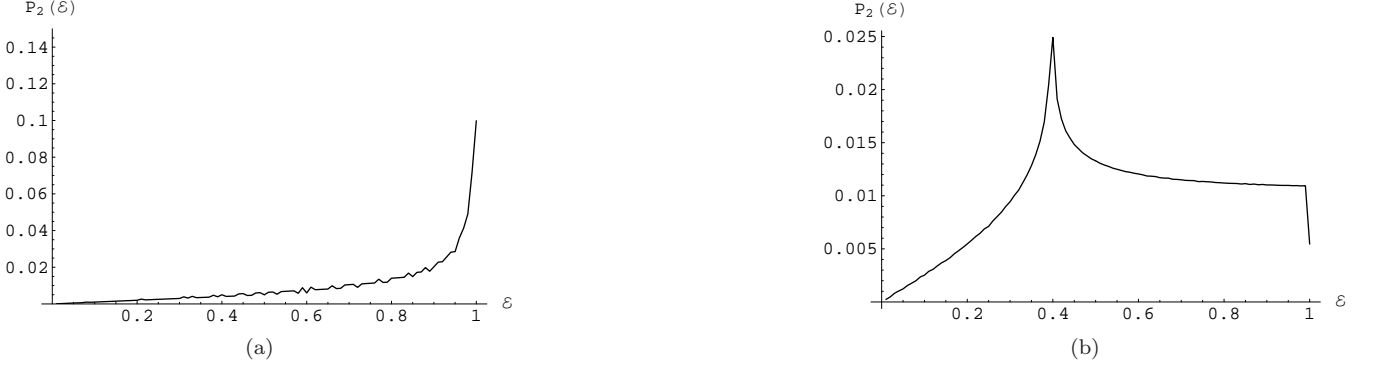


FIG. 6: The density function $\mathcal{P}_2(\mathcal{E})$ with respect to the entanglement \mathcal{E} for an evolution time $t = 2.0$, $T = 5.0$ and bath squeezing parameter r equal to 0.2. Figure (a) refers to the independent decoherence model and (b) to the collective decoherence model.

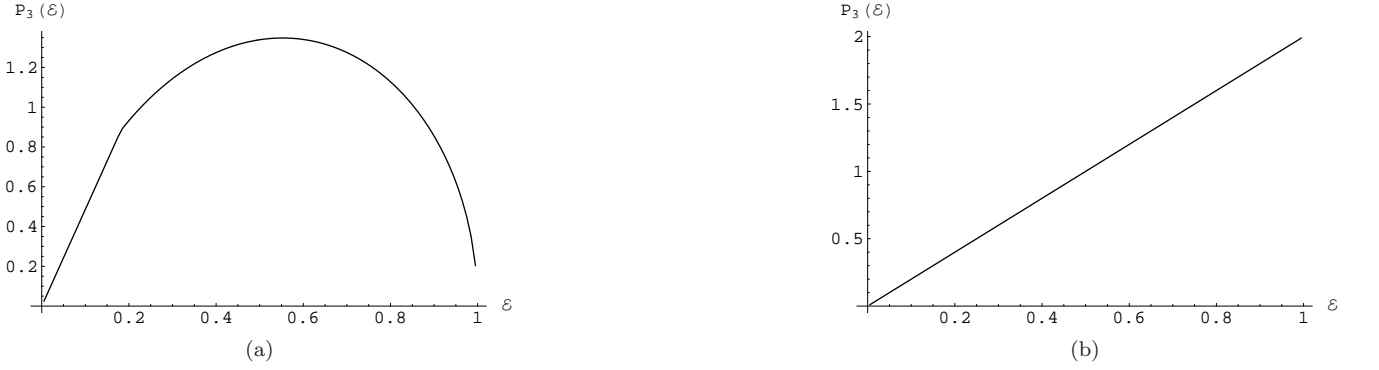


FIG. 7: The density function $\mathcal{P}_3(\mathcal{E})$ with respect to the entanglement \mathcal{E} for an evolution time $t = 2.0$, $T = 5.0$ and bath squeezing parameter r equal to 0.2. Figure (a) refers to the independent decoherence model and (b) to the collective decoherence model.

resist randomization. Such a state of affairs would be encountered if the effect of the bath is not a counterpart of the collision term (in a Boltzmann equation), but is more like a Vlasov term, causing long range mean field contributions [41].

From the numerical results, it is seen that the effect of the bath can be mapped to a T dependent effective hamiltonian whose energy eigenvalues scale with temperature. The eigenstates are given by the standard Bell states with the ground state being $|B_1\rangle = \frac{1}{\sqrt{2}}(|01\rangle + |10\rangle)$ while the orthogonal singlet state ($|B_4\rangle = \frac{1}{\sqrt{2}}(|01\rangle - |10\rangle)$) is the

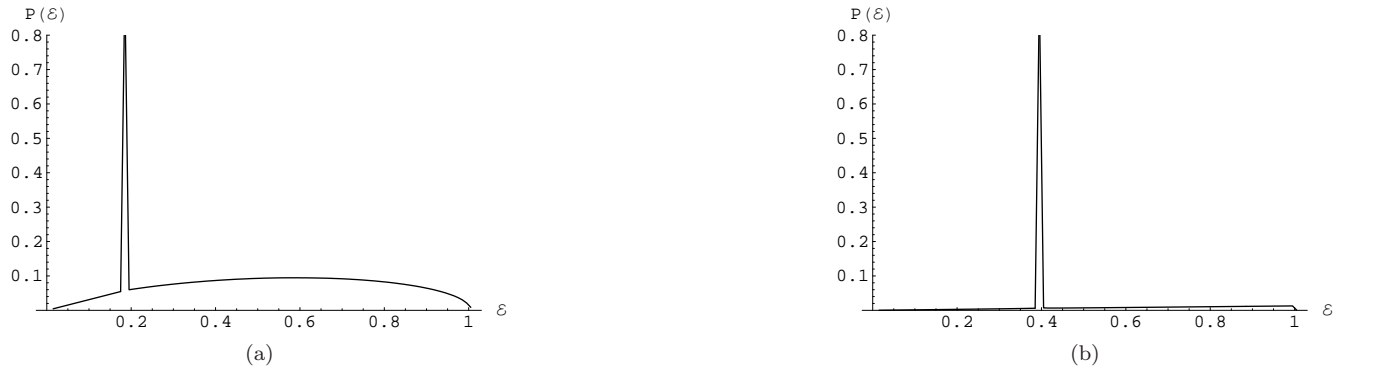


FIG. 8: The full density function $\mathcal{P}(\mathcal{E})$ (3) with respect to the entanglement \mathcal{E} for an evolution time $t = 2.0$, $T = 5.0$ and bath squeezing parameter r equal to 0.2. Figure (a) refers to the independent decoherence model and (b) to the collective decoherence model.

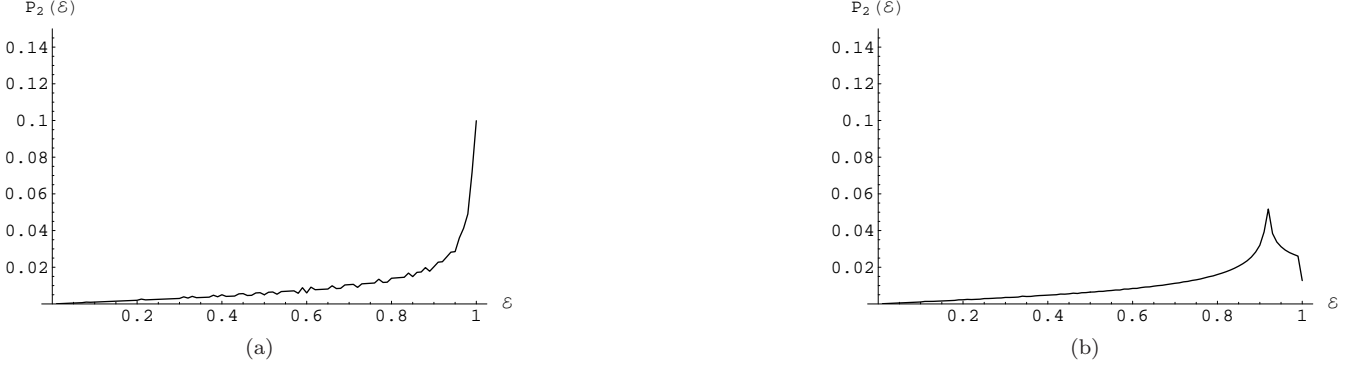


FIG. 9: The density function $\mathcal{P}_2(\mathcal{E})$ with respect to the entanglement \mathcal{E} for an evolution time $t = 10.0$, $T = 5.0$ and bath squeezing parameter r equal to 0.2. Figure (a) refers to the independent decoherence model and (b) to the collective decoherence model.

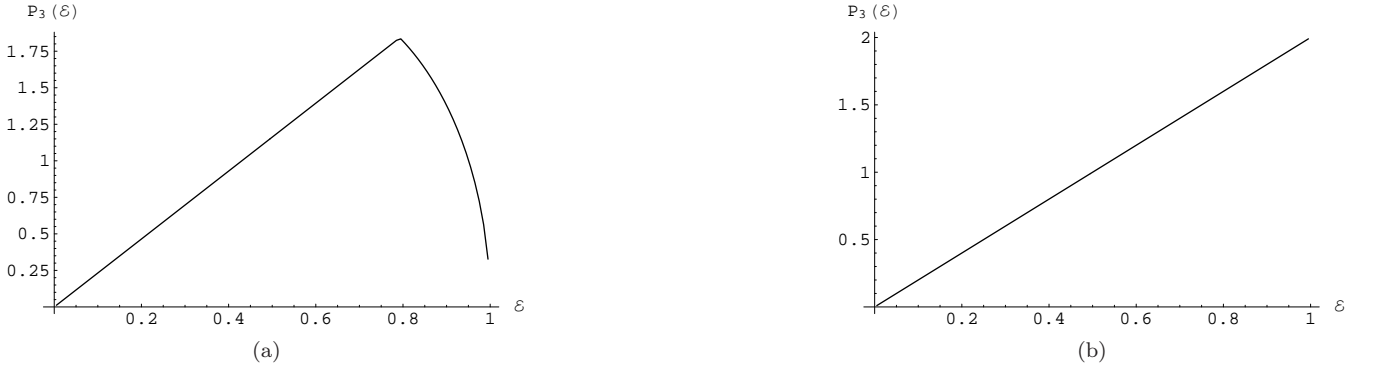


FIG. 10: The density function $\mathcal{P}_3(\mathcal{E})$ with respect to the entanglement \mathcal{E} for an evolution time $t = 10.0$, $T = 5.0$ and bath squeezing parameter r equal to 0.2. Figure (a) refers to the independent decoherence model and (b) to the collective decoherence model.

highest energy state, and is practically decoupled (with no population). The next excited state is degenerate, with two Bell states ($|B_2\rangle = \frac{1}{\sqrt{2}}(|00\rangle - |11\rangle)$, $|B_3\rangle = \frac{1}{\sqrt{2}}(|00\rangle + |11\rangle)$) spanning the two dimensional subspace. The effective temperature dependent hamiltonian is given by

$$H_{\text{eff}} = \sum_{i=1}^4 E_i(\beta) |B_i\rangle \langle B_i|,$$

where $|B_1\rangle$, $|B_2\rangle \langle B_2| + |B_3\rangle \langle B_3| = |00\rangle \langle 00| + |11\rangle \langle 11|$ and $|B_4\rangle$ are the Bell states, as defined above, with eigenvalues $\lambda_1 = 0.5$, $\lambda_2 = \lambda_3 = 0.25$ and $\lambda_4 \approx 0$, respectively. Since the Bell states are completely entangled, the effective hamiltonian has no linear terms in the qubit polarizations and has the form

$$H_{\text{eff}} \sim \frac{\ln(2)}{2\beta} (1 - (-\sigma_x^{(1)} \sigma_x^{(2)} + \sigma_y^{(1)} \sigma_y^{(2)} - \sigma_z^{(1)} \sigma_z^{(2)})) + \frac{\ln(4)}{\beta} \left(\frac{1}{2} + 2\sigma_z^{(1)} \sigma_z^{(2)} \right), \quad (62)$$

in writing which the singlet term has been dropped, as it is energetically very far separated from the other three levels. The above analysis places in perspective the surprising result that although the system is evolving, through the effective Hamiltonian, the entanglement density function remains practically restricted to the 3-dimensional subspace, with a large contribution from a Bell state, as a signal to the 3-dimensional background. The restriction of the effective dynamics from four to three levels is also seen in the case of two qubit evolution via a dissipative $S - R$ interaction with a thermal bath initially at $T = 0$ [42], for the collective decoherence model. However, there the reason for it is simply given by the fact that for the above conditions, the coupling term connecting one of the levels to the others goes to zero, thereby reducing the dynamics to that between three levels.

An interesting analog of the discussion in this Section comes in the work presented in [43]. There it was shown by the authors that for the scenario where there exists a system consisting of three subsystems with the first and the third

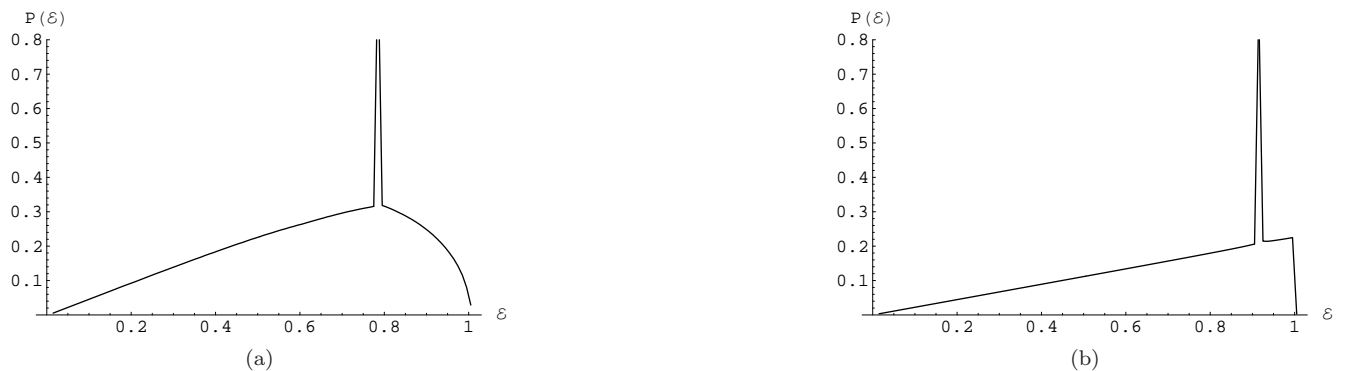


FIG. 11: The full density function $\mathcal{P}(\mathcal{E})$ (3) with respect to the entanglement \mathcal{E} for an evolution time $t = 10.0$, $T = 5.0$ and bath squeezing parameter r equal to 0.2. Figure (a) refers to the independent decoherence model and (b) to the collective decoherence model.

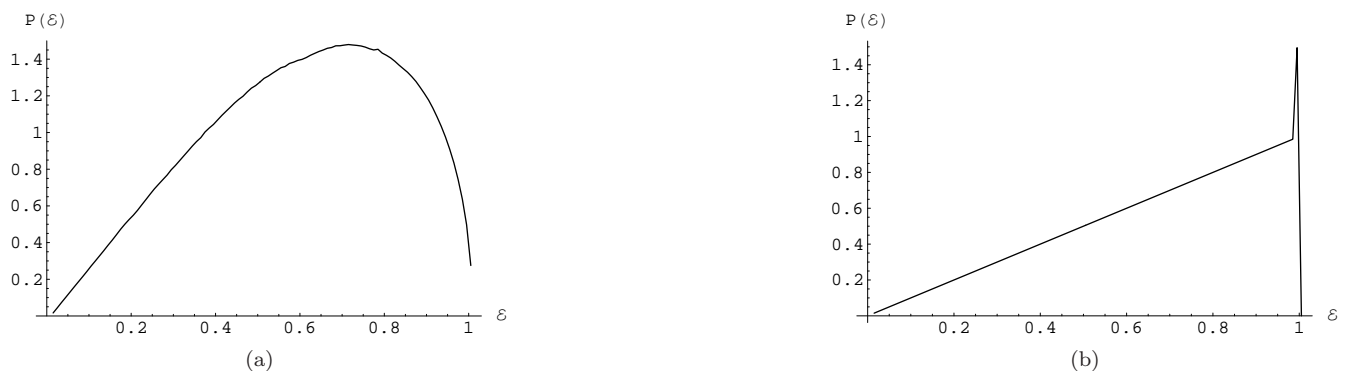


FIG. 12: The full density function $\mathcal{P}(\mathcal{E})$ (3) with respect to the entanglement \mathcal{E} for an evolution time $t = 10.0$, $T = 50.0$ and bath squeezing parameter r equal to 0.2. Figure (a) refers to the independent decoherence model and (b) to the collective decoherence model.

interacting with each other via their interactions with the mediating second subsystem, a signature of entanglement between the first and the third subsystems is the degeneracy in the ground state of the system. Here we have a similar situation with the two qubits interacting with a bath which in turn mediates the inter-qubit interaction. From our effective Hamiltonian H_{eff} , we see that the first excited state (not the ground state), spanned by the Bell states $|B_2\rangle$ and $|B_3\rangle$, is degenerate and the system exhibits a strong entanglement even at finite temperatures. Another work by the same authors [44], studied the persistence of mixed state entanglement at finite T . This would be important as quantum effects can be expected to dominate in regions where entanglement is nonzero. They considered the transverse Ising model and studied the two-site entanglement, using concurrence as the entanglement measure, and found appreciable entanglement in the system at finite T above the ground state energy gap, one of their motivations being the influence of nearby critical points to the finite T entanglement. The persistence of entanglement in a two-qubit system interacting with the bath via a purely dephasing interaction (QND) would suggest a broad applicability of these concepts, thereby highlighting the interconnection of ideas of quantum information to quantum statistical mechanics.

VIII. AN APPLICATION TO QUANTUM COMMUNICATION: QUANTUM REPEATERS

We now make an application of the two-qubit reduced dynamics obtained from QND system-reservoir interaction to a quantum repeater [31], used for quantum communication over long distances. The efficiency of quantum communication over long distances is reduced due to the effect of noise, which can be considered as a natural open system effect. For distances much longer than the coherence length of a noisy quantum channel, the fidelity of transmission is usually so low that standard purification methods are not applicable. In a quantum repeater set-up, the channel is divided into shorter segments that are purified separately and then connected by the method of entanglement swapping, which

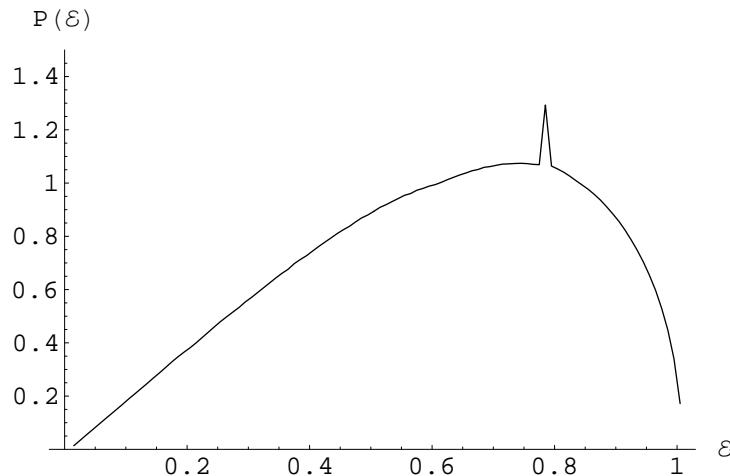


FIG. 13: The full density function $\mathcal{P}(\mathcal{E})$ (3) with respect to the entanglement \mathcal{E} for the independent decoherence model with an evolution time $t = 10.0$, $T = 20.0$ and bath squeezing parameter r equal to 0.2.

is the quantum teleportation [45] of entanglement. This method can be much more efficient than schemes based on quantum error correction, as it makes explicit use of two-way classical communication. The quantum repeater system allows entanglement purification over arbitrary long channels and tolerates errors on the percent level. It requires a polynomial overhead in time, and an overhead in local resources that grows only logarithmically with the length of the channel.

Here we consider the effect of noise, introduced by imperfect local operations that constitute the protocols of entanglement swapping and purification [32], on such a compound channel, and how it can be kept below a certain threshold. The noise process studied is the one obtained from the two-qubit reduced dynamics via a QND interaction, instead of the depolarizing noise considered in [31]. A detailed study of the effect of the two-qubit noise on the performance of a quantum repeater is underway and will be reported elsewhere. Here we treat this problem in a simplified fashion, and study the applicability and efficiency of entanglement purification protocols in the situation of imperfect local operations.

A quantum repeater involves the two tasks of entanglement swapping, involving Bell-state measurements, and entanglement purification, involving CNOT gates. The Bell-state measurement may be equivalently replaced by a CNOT followed by a projective single-qubit measurement. In entanglement swapping, two distant parties initially not sharing entanglement with each other, but sharing entanglement separately with a third party, become entangled by virtue of a multi-partite measurement by the third party on the latter's two halves of entanglement. Entanglement purification involves two parties employing local operations and classical communication (LOCC) to improve the fidelity F of Einstein-Podolsky-Rosen (EPR) pairs they share, with respect to a maximally entangled state. The local operations involve two-qubit gates such as the CNOT operation, followed by single qubit measurement, and a possible discarding of an EPR pair. Provided $F > 0.5$, and at the cost of losing shared (impure) entanglement, the two parties can increase the fidelity of the remaining shared entanglement to

$$F' = \frac{F^2 + [(1 - F)/3]^2}{F^2 + [2F(1 - F)/3] + (5/9)(1 - F)^2}, \quad (63)$$

where F and F' are, respectively, the input and output fidelities of the entanglement purification protocol proposed by Bennett *et al.* [32].

In the simplified scenario we consider, the output of the noisy CNOT is taken to be a mixed separable state, in place of a pure separable state that is obtained in the noiseless case. As a further simplification, in order to facilitate an easy connection with the purification protocol due to Bennett *et al.*, this mixed state is assumed to be of the form:

$$\rho(F) = F^2|+, +\rangle\langle+, +| + (1 - F^2)|-, -\rangle\langle-, -|, \quad (64)$$

where we use the notation $|\pm\rangle = (1/\sqrt{2})(|\frac{1}{2}\rangle \pm |-\frac{1}{2}\rangle)$, and $|\pm, \pm\rangle \equiv |\pm\rangle \otimes |\pm\rangle$. Thus, $\rho(F)$ is a mixture in the two dimensional space spanned by $\{|+, +\rangle, |-, -\rangle\}$, parametrized by fidelity F , given by $\sqrt{\langle+, +|\rho(F)|+, +\rangle}$. In the notation of Section IV A, these basis states are $\frac{1}{2}(|0\rangle + |1\rangle + |2\rangle + |3\rangle)$ and $\frac{1}{2}(|0\rangle - |1\rangle - |2\rangle + |3\rangle)$. The state $\rho(F)$ is then the input to the purification protocol, whereby we obtain the output fidelity F' as a function of F .

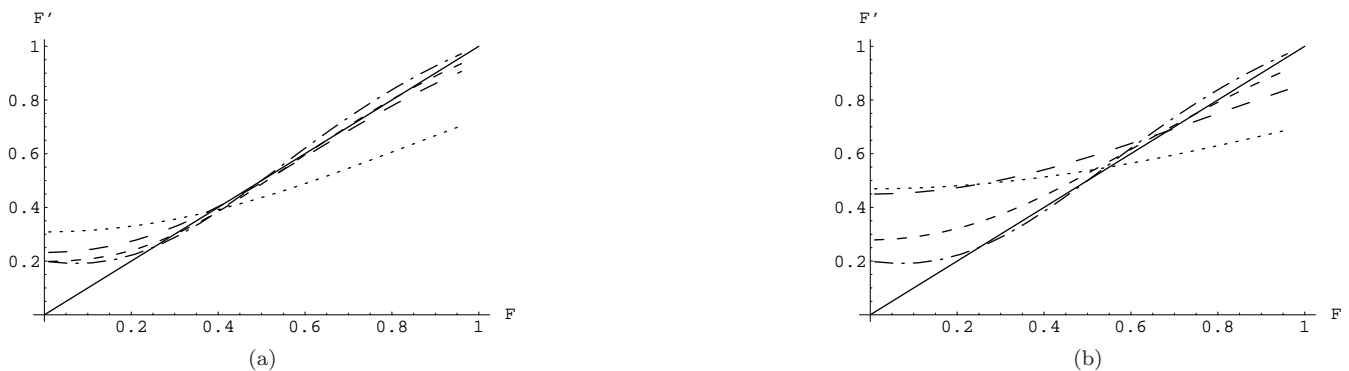


FIG. 14: Purification loop for connecting and purifying EPR pairs. The noisy channel is modelled as a two-qubit QND interaction with the environment in the independent ($kr_{ab} \geq 1$) (plot (a)) and collective ($kr_{ab} \ll 1$) (plot (b)) decoherence regime, with the input state given by $\rho(F)$ in Eq. (64), where r_{ab} is the inter-qubit distance. The bold line is the $F = F'$ plot, the small and large dashed curves represent $T = 2$ and bath squeezing parameter (Eq. (20)) $r = 0.5$, with $t = 3$ and 5 , respectively. The dotted line represents $t = 5, T = 2, r = 1.5$, while the dot-dashed curve is due to the noiseless Bennett et al. protocol.

We depict in figures (14(a)) and (b) the modified ‘purification loop’, obtained by subjecting the noiseless loop to the above model of noise. In all cases in both figures, as expected, we find that noise degrades the performance of the purification protocol. To evaluate the performance, it may be compared with the noiseless case, given by the dot-dashed curve in both figures. That this curve lies above the $F = F'$ line in the closed range $[0.5, 1]$ implies that fidelities above the minimum value $F_{\min} = 0.5$ can be corrected to the maximum value $F_{\max} = 1$ by repeated application of purification. The degrading effect of noise can be seen in two ways: it introduces an off-set, whereby an input of $F = 1$ does not yield the same output and restricts F_{\max} to values less than 1.

In both figures, comparison of the small and large dashed curves shows that increasing bath exposure time degrades the fidelity by suppressing F_{\max} (the point where a curve cuts the $F = F'$ line from above) and increasing the off-set at $F = 1$. A comparison of large-dashed and dotted curves brings out a similar degrading effect of increasing bath squeezing. A similar effect can be shown for temperature. The surprise that emerges in comparing the collective and independent decoherence models is that, contrary to expectation, the latter produces a less damaging effect on purification than the former.

IX. CONCLUSIONS

In this article, we have analyzed in detail the dynamics of entanglement in a two-qubit system interacting with its environment via a QND $S - R$ interaction. The system and reservoir are initially assumed to be separable with the reservoir being in an initial squeezed thermal state. Since the resulting dynamics becomes mixed, in order to analyze the ensuing entanglement, we have made use of a recently introduced measure of mixed state entanglement via a PDF. This enables us to give a statistical and geometrical characterization of entanglement.

After developing the general dynamics of N qubits interacting with their bath (reservoir) via a QND $S - R$ interaction, we specialized to the two-qubit case for applications. Due to the position dependent coupling of the qubits with the bath, the dynamics could be naturally divided into an independent and collective decoherence regime, where in the collective decoherence regime, the qubits are close enough to feel the bath collectively. We analyzed the open system dynamics of the two qubits, both for the independent as well as the collective regimes and saw that in the collective regime, there emerges the possibility of a decoherence-free subspace for the case of zero bath squeezing. Interestingly, the dynamics was found to obey two symmetry operations: hermiticity and spin-flip symmetries. The existence of the nontrivial spin-flip symmetry would explain the emergence of a decoherence-free subspace (DFS) [46], thereby providing a concrete instance of a DFS.

We then made an analysis of the two-qubit entanglement for different bath parameters. We analyzed both concurrence as well as the PDF by finding the entanglement content of the various subspaces that span the two-qubit Hilbert space. Although the PDF agrees in its predictions with concurrence, it is able to extract more information out of the system as a result of its statistical-geometrical nature. Thus we were able to consider an example analogous to NMR quantum computation, wherein the concurrence would be zero, and the excess of entangled states over the unpolarized background is exploited as a resource allowing for non-trivial quantum information processing. For the

collective decoherence model the PDF for the full density function exhibits a rich entanglement structure, coming principally from the contributions from the one and three dimensional projections which carry equal weights thereby suggesting a tendency of the system to resist randomization. This feature is seen to persist even for higher temperatures and evolution times with the weights of the subspaces spanned by the four projection operators of the PDF remaining intact, thereby enabling us to give an effective T dependent dynamics in the collective decoherence regime. A comparison of this with some related works suggests the applicability of quantum information theoretic ideas to quantum statistical mechanical systems. Finally we made an application to a simplified model of a quantum repeater, which can be adapted for quantum communication over long distances.

Acknowledgments

We wish to thank Shanthanu Bhardwaj for numerical help.

-
- [1] W. H. Louisell, *Quantum Statistical Properties of Radiation* (John Wiley and Sons, 1973).
 - [2] A. O. Caldeira and A. J. Leggett, *Physica A* **121**, 587 (1983).
 - [3] W. H. Zurek, *Phys. Today* **44**, 36 (1991); *Prog. Theor. Phys.* **87**, 281 (1993).
 - [4] S. Banerjee and R. Ghosh, *J. Phys. A: Math. Theo.* **40**, 13735 (2007); eprint quant-ph/0703054.
 - [5] V. B. Braginsky, Yu. I. Vorontsov and K. S. Thorne, *Science* **209**, 547 (1980).
 - [6] V. B. Braginsky and F. Ya. Khalili, in *Quantum Measurements*, edited by K. S. Thorne (Cambridge University Press, Cambridge, 1992).
 - [7] D. F. Walls and G. J. Milburn, *Quantum Optics* (Springer, Berlin, 1994).
 - [8] W. H. Zurek, in *The Wave-Particle Dualism*, edited by S. Diner, D. Fargue, G. Lochak and F. Selleri (D. Reidel Publishing Company, Dordrecht, 1984).
 - [9] C. M. Caves, K. D. Thorne, R. W. P. Drever, V. D. Sandberg and M. Zimmerman, *Rev. Mod. Phys.* **52**, 341 (1980).
 - [10] M. F. Bocko and R. Onofrio, *Rev. Mod. Phys.* **68**, 755 (1996).
 - [11] C. J. Myatt, B. E. King, Q. A. Turchette, C. A. Sackett, *et al.*, *Nature* **403**, 269 (2000).
 - [12] Q. A. Turchette, C. J. Myatt, B. E. King, C. A. Sackett, *et al.*, *Phys. Rev. A* **62**, 053807 (2000).
 - [13] G. J. Pryde, J. L. O'Brien, A. G. White, *et al.*, *Phys. Rev. Lett.* **92**, 190402 (2004); J. L. O'Brien, G. J. Pryde, A. G. White, *et al.*, *Nature* **426**, 264 (2003).
 - [14] R. Onofrio and L. Viola, *Phys. Rev. A* **58**, 69 (1998).
 - [15] J. S. Bell, *Physics* **1**, 195 (1964).
 - [16] M. Nielsen and I. Chuang, *Quantum Computation and Quantum Information* (Cambridge University Press, Cambridge, 2000).
 - [17] P. Shor, *SIAM Journal of Computing* **26**, 1484 (1997); L. K. Grover, *Phys. Rev. Lett.* **79**, 325 (1997).
 - [18] S. Calderbank and P. Shor, *Phys. Rev. A* **54**, 1098 (1996); A. Steane, *Proc. Roy. Soc., London, Ser. A* **452**, 2551 (1996).
 - [19] A. Beige, D. Braun, B. Tregenna and P. L. Knight, *Phys. Rev. Lett.* **85**, 1762 (2000).
 - [20] M. Fleischhauer, S. F. Yelin and M. D. Lukin, *Opt. Commun.* **179**, 395 (2000).
 - [21] S. Schneider and G. J. Milburn, *Phys. Rev. A* **65**, 042107 (2002).
 - [22] H.-P. Breuer and F. Petruccione, *The Theory of Open Quantum Systems* (Oxford University Press 2002).
 - [23] H. Carmichael, *An Open Systems Approach to Quantum Optics* (Springer 1993).
 - [24] M. P. Almeida, F. de Melo, M. Hor-Meyll, A. Salles, *et al.*, *Science* **316**, 579 (2007); A. Salles, F. Melo, M. P. Almeida, M. Hor-Meyll, *et al.*, arXiv:0804.4556.
 - [25] R. Srikanth and S. Banerjee, *Phys. Rev. A* **77**, 012318 (2008); arXiv:0707.0059.
 - [26] C. H. Bennett, D. P. DiVincenzo, J. A. Smolin and W. K. Wootters, *Phys. Rev. A* **54**, 3824 (1996).
 - [27] W. K. Wootters, *Phys. Rev. Lett.* **80**, 2245 (1998).
 - [28] F. Mintert, A. R. R. Carvalho, M. Kus and A. Buchleitner, *Phys. Reports* **415**, 207 (2005).
 - [29] R. F. Werner, *Phys. Rev. A* **40**, 4277 (1989).
 - [30] S. Bhardwaj and V. Ravishankar, *Phys. Rev. A* **77**, 022322 (2008).
 - [31] H.-J. Briegel, W. Dür, J. I. Cirac and P. Zoller, *Phys. Rev. Lett.* **81**, 5932 (1998); W. Dür, H.-J. Briegel, J. I. Cirac, and P. Zoller, *Phys. Rev. A* **59**, 169 (1999).
 - [32] C. H. Bennett, G. Brassard, S. Popescu, B. Schumacher *et al.*, *Phys. Rev. Lett.* **76**, 722 (1996).
 - [33] J. H. Reina, L. Quiroga and N. F. Johnson, *Phys. Rev. A* **65**, 032326 (2002).
 - [34] S. Banerjee, J. Ghosh and R. Ghosh, *Phys. Rev. A* **75**, 062106 (2007); eprint quant-ph/0703055.
 - [35] S. Banerjee and R. Srikanth, *Eur. Phys. J. D* **46** 335 (2008); eprint quant-ph/0611161.
 - [36] C. M. Caves and B. L. Schumacher, *Phys. Rev. A* **31**, 3068 (1985); B. L. Schumacher and C. M. Caves, *Phys. Rev. A* **31**, 3093 (1985).
 - [37] B. L. Hu and A. Matacz, *Phys. Rev. D* **49**, 6612 (1994).
 - [38] S. Banerjee, *Physica A* **337**, 67 (2004).

- [39] S. Banerjee and J. Kupsch, *J. Phys. A: Math. Gen.* **38**, 5237 (2005).
- [40] T. E. Tilma, M. Byrd and E. C. G. Sudarshan, *J. Phys. A: Math. Gen.* **35**, 9255 (2002).
- [41] E. Carlen, R. Esposito, J. L. Lebowitz, R. Marra and A. Rokhlenko, Preprint (1994) (unpublished).
- [42] Z. Ficek and R. Tanaś, *Physics Reports*, **372**, 369 (2002).
- [43] H. L. Haselgrove, M. A. Nielsen and T. J. Osborne, arXiv:quant-ph/0308083.
- [44] T. J. Osborne and M. A. Nielsen, arXiv:quant-ph/0202162.
- [45] C. H. Bennett, G. Brassard, C. Crépeau, R. Josza, A. Peres and W. K. Wootters, *Phys. Rev. Lett.* **70**, 1895 (1993).
- [46] P. Zanardi and M. Rasetti, *Phys. Rev. Lett.* **79**, 3306 (1998); L. M. Duan and G. C. Guo, *Phys. Rev. A* **57**, 737 (1998); D. A. Lidar, I. L. Chuang and K. B. Whaley, *Phys. Rev. Lett.* **89**, 2594 (1998); D. A. Lidar and K. B. Whaley, *Irreversible Quantum Dynamics*, F. Benatti and R. Floreanini (eds.) *Springer Lecture Notes in Physics* **622** (Berlin 2003).